Available online at www.sciencedirect.com

ScienceDirect

Procedia Engineering 100 (2015) 384 – 393

Procedia Engineering

www.elsevier.com/locate/procedia

25th DAAAM International Symposium on Intelligent Manufacturing and Automation, DAAAM 2014

Experimental and Numerical Investigation of Temperature Distribution and Hole Geometry during Laser Drilling Process

Derzija Begic-Hajdarevic*, Izet Bijelonja

Faculty of Mechanical Engineering, University of Sarajevo, Vilsonovo setaliste 9, Sarajevo 71000, Bosnia and Herzegovina

Abstract

This paper reports on a numerical and experimental investigation of laser drilling of tungsten alloy for modeling the temperature distribution to predict the heat affected zone (HAZ) and the shape of the hole. The numerical method is based on the solution of the integral form of the thermal energy equation, expressed in terms of temperature via corresponding constitutive relation, and discretized by the finite volume method. The method has been applied to a number of test cases and the results are compared with the experimental data. It was observed that the finite volume method results were in good agreement with experimental data and that it can be used as useful tool for predicting heat affected zone and the shape of the hole during laser drilling process.

Peer-review under responsibility of DAAAM International Vienna

Keywords: laser drilling; finite volume method; tungsten alloy; temperature distribution; process parameters

1. Introduction

During the laser beam machining, the laser beam focused on the surface of the part causes the rapid heating of the material until the fusion. Molten metal is then ejected by using a gas jet of high pressure. Due to the complexity of laser processes, where a variety of different physical phenomena are coupled with each other, their modeling and simulation remains a difficult task despite of strong efforts of scientists in the past [1]. Modeling and simulation of the laser beam machining is indispensable for optimization purposes. Modeling can be done by implementing analytical, numerical and experimental methods.

* Corresponding author. Tel.: +387-33-729-881; fax: +387-33-653-055.
E-mail address: begic@mef.unsa.ba

Peer-review under responsibility of DAAAM International Vienna
doi:10.1016/j.proeng.2015.01.382

Numerical process simulations are of great importance both for industry and science. In science, simulations enable for a thorough process understanding as it is possible to separate different processes or material parameters in their effect on the machining result. In industrial production, simulations serve as a tool for planning of single production steps or even of whole process chains. A thermal model to describe the temperature profile and thermal stress propagation for laser drilled holes in high purity fired alumina ceramic considering a continuous, distributed, and moving heat source has developed in [2]. Using the finite element method the shape of ultrasonic aided laser drilled holes and thickness of the recast layer are determined [3]. A 2D axisymmetric model based on the volume of fluid approach is developed to analyze quantitatively the influence of the fluid flow and heat transfer in the transient development of a laser drilled hole in a turbine airfoil material [4]. In [5] is described a 3D finite difference based heat flow model for the prediction of the shape of hole and size in carbon fibre composites during laser drilling. A 1D thermal model for the prediction of erosion depth in ceramics during pulsed Nd:YAG laser drilling considering the absorption of plasma plume formed on the surface of the ceramics is presented in [6]. A 2D numerical model based on the finite volume method used in [7] to predict the temperature distribution during laser drilling process. A two-dimension axisymmetric finite element model for simulation of temperature field and proceeding of hole formation during percussion drilling was developed in [8]. The study indicated that the size and temperature of the melt front significantly affected the hole diameter formation and spatter deposition during laser percussion drilling. For modeling and optimization of laser beam percussion drilling of nickel-based super alloy sheet [9] and thin aluminum sheet [10] is developed a 2D axisymmetric finite element method based thermal model. Amongst the numerical methods, the finite element method is the most common [11].

The present paper aims to show the finite volume method application to the mathematical model of a laser drilling process. The model is applied to determine temperature distribution to predict the heat affected zone and hole geometry in laser drilling of tungsten alloy sheet thickness of 1 mm. Finally, the numerical results are compared by the self-conducted experimental data.

2. Mathematical formulation

In this section the mathematical model for prediction of temperature distribution during laser drilling process is presented. It includes an integral form of the thermal energy equation, constitutive relation, and initial and boundary conditions.

An integral form of the thermal energy balance equation is given by:

$$\frac{\partial}{\partial t}\int_V \rho c T dV = \int_S \mathbf{q}\cdot\mathbf{n}\, dS + \int_V h_S\, dV, \tag{1}$$

which is valid at all instants of time t for an arbitrary part of continuum of volume V bounded by the surface S with normal vector $\mathbf{n}$ pointing outwards. In Eq. (1), ρ is the material density, c is the specific heat, T is the temperature, $\mathbf{q}$ is the heat flux vector, h_S is the sink of heat which simulates the latent heat in the case of laser drilling process.

The constitutive relation between the heat flux and temperature gradient is given by Fourier's law:

$$\mathbf{q} = k \operatorname{grad} T, \tag{2}$$

where k is the thermal conductivity.

To complete the mathematical model, initial and boundary conditions have to be specified. As initial conditions, the temperature has to be specified at all points of the solution domain. Boundary conditions have to be specified at all times at all solution domain boundaries. They can be either of Dirichlet type (temperature) or of Neumann type (heat flux).

3. Numerical procedure

The governing equation, together with non-linear boundary conditions, applied to the two-dimensional drilling geometry is solved using finite volume method. As all numerical methods, it consists of time, space and equations discretization.

3.1. Discretization

In order to obtain discrete counterparts of Eq. (1), the time is discretized into an arbitrary number of time steps δt and the solution domain is subdivided into a finite number of contiguous quadrilateral controls volumes (CV) or cells of volume V bounded by six cell faces of the surface S_f ($f = w, e, s, n, d, u$), see Fig. 1. The computational points (nodes) are placed at the center of each CV, while boundary nodes, needed for the specification of boundary conditions, reside at the center of the boundary cell faces.

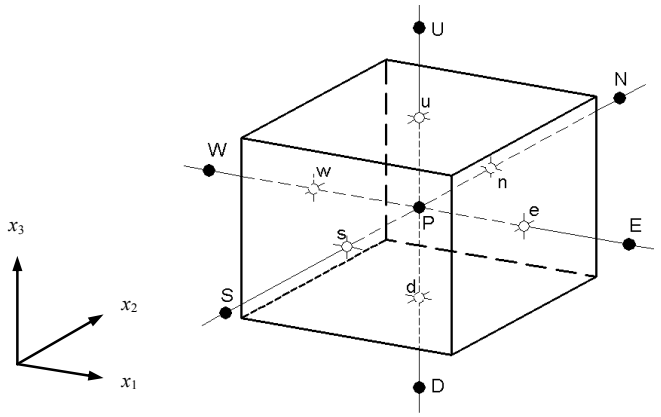

Fig. 1. Control volume of node P and the neighboring nodes E, W, S, N, U, D.

Introducing constitutive relation (2) into energy balance equation (1) and after the space discretization, the energy balance equation is written for each control volume as follows:

$$\underbrace{\frac{\partial}{\partial t}\int_V \rho c T dV}_{\text{Rate of change}} = \underbrace{\sum_f \int_{S_f} k\ \text{grad}\, T \cdot \mathbf{n}\, dS}_{\text{Diffusion}} + \underbrace{\int_V h_S\, dV}_{\text{Source term}}\ (f = w, e, s, n, d, u), \tag{3}$$

where f is the number of faces enclosing the cell P (in this case $f = 6$, see Fig. 1), V is the control volume and S_f is the surface of cell-face f. In order to evaluate integrals in the above equation, a distribution of dependent variable in space and time have to be approximated.

Using the backward differencing in time and the midpoint rule, the rate of change term is approximated as:

$$\frac{\partial}{\partial t}\int_V \rho c T dV \approx \frac{1}{\delta t_m}\left[(\rho c T V)_P^m - (\rho c T V)_P^{m-1}\right], \tag{4}$$

where the superscripts m and $(m - 1)$ denote values at the *current* and *previous* instants of time separated by the time interval δt_m, and subscript P refers to the cell P.

Again using the midpoint rule and assuming a linear variation of the dependent variable T between the neighboring nodes, the diffusion term is approximated as:

$$\sum_f \int_{S_f} k \operatorname{grad} T \cdot \mathbf{n}\, dS \approx \sum_f \left(k \frac{S}{\delta x_j} \right)_f \left[\Delta T \right]_f \quad (f = w, e, s, n, d, u), \tag{5}$$

where there is no summation on j ($j = 1$ for $f = w$, e, $j = 2$ for $f = s$, n and $j = 3$ for $f = d$, u) and where at the west cell face, for example

$$\left(k \frac{S}{\delta x_j} \right)_w \left[\Delta T \right]_w = -\left(k \frac{S}{\delta x_1} \right)_w \left(T_P - T_W \right) \tag{6}$$

where subscript w denotes values at the west cell face (δx_{1w} is the distance between nodes P and W) and T_P and T_W are values of the temperature at the corresponding cell centers at the new time level. This implies that a fully implicit differencing scheme is used together with a second order spatial differencing scheme to express the cell-face values of dependent variable in terms of the neighboring nodal values.

The source term is approximated by using the midpoint rule:

$$\int_V h_S dV \approx h_{SP} V_P, \tag{7}$$

where h_{SP} is the sink of heat at the node P and V_P is the cell volume.

As a consequence of the above approximations, equation (3) can be written in the following form:

$$a_P T_P - \sum_F a_F T_F = b \quad (F = W, E, S, N, D, U), \tag{8}$$

Where summation is to be performed over all six cells neighboring cell P, and coefficients a_F have the following form:

$$\begin{aligned} a_F &= \left(k \frac{S}{\delta x_j} \right)_f, \quad F = W, E, S, N, D, U, \quad f = w, e, s, n, d, u, \quad j = \begin{cases} 1 & \text{for} \quad f = w, e, \\ 2 & \text{for} \quad f = s, n, \\ 3 & \text{for} \quad f = d, u, \end{cases} \\ a_P &= \sum_F a_F + \left\{ \frac{1}{\delta t_m} \left(\rho c V \right)_P \right\} \\ b &= h_{SP} V_P + \left\{ \frac{1}{\delta t_m} \left(\rho c T V \right)_P^{m-1} \right\}, \end{aligned} \tag{9}$$

where all variables in Eq. (9) are refer to the current time, unless indicated otherwise.

It is important to note that for any discretization of space and time, a_F is always non-negative, which implies

$$\left| a_P \right| \geq \sum_F \left| a_F \right| \quad (F = W, E, S, N, D, U). \tag{10}$$

Thus, as a result of the discretization procedure employed, a set of N non-linear algebraic equations of the form (8) with nodal values of temperature as unknowns is obtained, where N is the number of CVs. The set of equations is then solved by an iterative procedure.

3.2. Initial and boundary condition

To start calculation, the initial value of temperature is required. On the faces coinciding with the boundary of the solution domain, boundary conditions have to be applied. On the boundary regions which are subjected to the effect of laser beam, the Neumann type boundary condition is defined as follows (inside of the laser beam):

$$k\frac{\partial T}{\partial n} = h\left(T_\infty - T\right) + \varepsilon\sigma\left(T_\infty^4 - T^4\right) + \alpha\, I(r,t), \tag{11}$$

where, h is the convection heat transfer, T_∞ is the environment temperature, T is the boundary temperature, ε is the emission coefficient, σ is the Stefan-Boltzmann constant, α is the absorption coefficient, I is the intensity of the incident laser beam. In this study, the radiation intensity is described by the Gaussian distribution, which corresponds to the TEM_{00} mode. In this case the intensity of the laser beam is given by [12]:

$$I(r,t) = \frac{2P}{\pi R_0^2}\exp\left(-\frac{2r^2}{R_0^2}\right), \tag{12}$$

where P is the laser power, R_0 is the radius of the focused laser beam, and r is the radial coordinate.

Boundary condition on the other boundary regions (outside of laser beam) is:

$$k\frac{\partial T}{\partial n} = h\left(T_\infty - T\right) + \varepsilon\sigma\left(T_\infty^4 - T^4\right). \tag{13}$$

4. Testing and application of the method

In order to demonstration the method, several examples are presented. First, the numerical results are demonstrated for different number of CVs, then for different time steps. After that, the temperature distribution and the shape of the drilled hole are presented for different times during laser drilling process. Finally, the numerical results are compared with the experimental data.

The thermo-physical properties of tungsten alloy, process parameters, and parameters important for the numerical calculation are shown in Table 1.

Table 1. Thermo-physical properties of sample and other parameters.

	Properties	Values
Tungsten alloy	T_L	3100 °C
	H_L	250 kJkg^{-1}
	α	0,86
	ρ	17600 kgm^{-3}
Other parameters	σ	5,67·10^{-8} Wm^{-2}K^{-4}
	h	25 Wm^{-2}K^{-1}
	P	1000 W
	t_t	8·10^{-3} s
	R_0	0,105 mm

T_L denotes the liquidus temperature, H_L is the latent heat and t_t is total drilling time. The emission coefficient ε, the thermal conductivity k, and the specific heat c are considered as temperature-dependent parameters for numerical calculation [13].

The spatial solution domain with boundary conditions for prediction of unsteady temperature fields into material during laser drilling process is shown in Fig. 2. In this case, the solution domain boundaries are variable due to the removal material from the machining zone. It makes problem nonlinear.

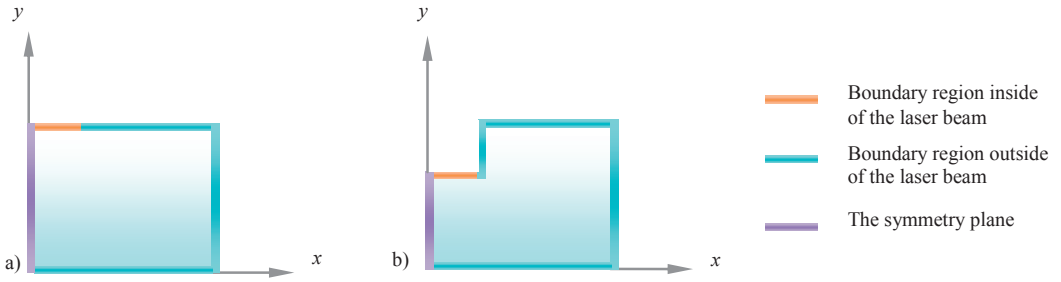

Fig. 2. (a) the initial solution domain; (b) the solution domain during drilling process.

The two-dimensional axis-symmetric model with the symmetry axis coinciding by the axis of the drilled hole is considered, see Fig.2. For numerical analysis used a sample of size 1,5 mm x 1 mm. The initial temperature of sample is the same as the environment temperature, while the boundary conditions are defined as follows:

$$\frac{\partial T}{\partial x} = 0 \qquad \text{- the symmetry plane,}$$

$$k\frac{\partial T}{\partial y} = h\left(T_\infty - T\right) + \varepsilon\sigma\left(T_\infty^4 - T^4\right) + \alpha I\left(r,t\right) \qquad \text{- boundary regions inside of the laser beam,}$$

$$k\frac{\partial T}{\partial n} = h\left(T_\infty - T\right) + \varepsilon\sigma\left(T_\infty^4 - T^4\right) \qquad \text{- boundary regions outside of the laser beam.}$$

The spatial solution domain is discretized by different number of control volumes. The drilled holes for different number of CVs are shown in Fig.3. Time step is 0.05 ms and the drilling time is 8 ms.

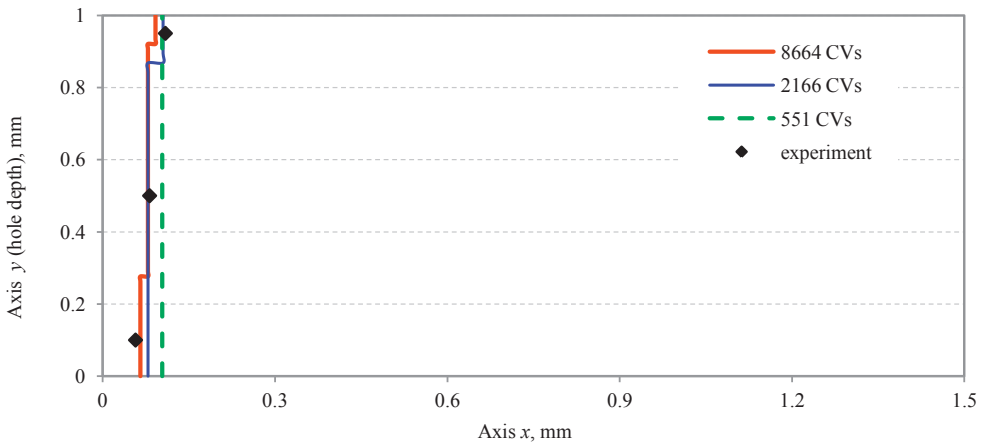

Fig. 3. The shape of drilled hole for different number CVs.

The temperature distribution into material, for coarse mesh of 551 CVs and fine mesh of 8664 CVs is illustrated in Fig.4.

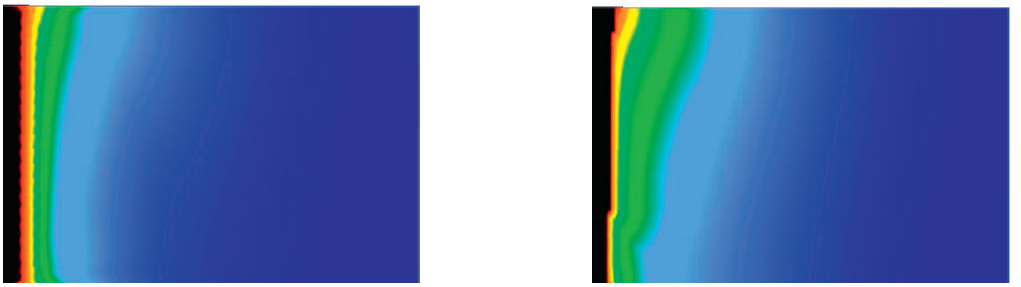

Fig. 4. Temperature distribution for different the number control volumes: 551 CVs (left) and 8664 CVs (right).

It can be concluded, there is difference between the numerical results for the coarse and fine mesh, see Figs. 3 and 4. The numerical results for drilled hole diameter are closest to the experiment for the finest computational mesh of 8664 CVs, and the largest difference between the numerical and experimental results is at the entrance of drilled hole and is approximately 13%. Further refinement of the computational mesh is not contributed significantly to a better quality of numerical results.

The numerical results of the drilled hole for different time steps is shown in Fig.5. Calculations were made for a fine mesh of 8664 CVs and three different time steps. Temperature distribution into material at the different time steps is illustrated in Fig.6. Drilled time is 2 ms.

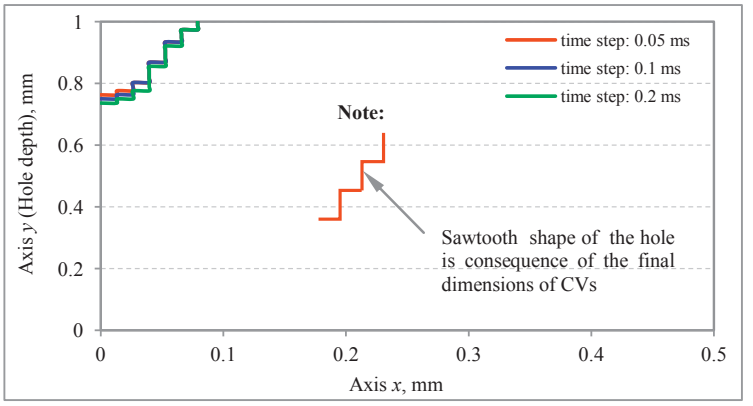

Fig. 5. The numerical drilled hole at different time steps.

Fig. 6. Temperature distribution at different time steps: 0.2 ms (left) and 0.05 ms (right).

It can be concluded that the difference in the numerical results for selected time steps is very small and is approximately 2%. The temperature distribution for the finest mesh 8664 CVs and the time step 0.05 ms during laser drilling at the times 1 ms, 2 ms and 4 ms is shown in Fig.7.

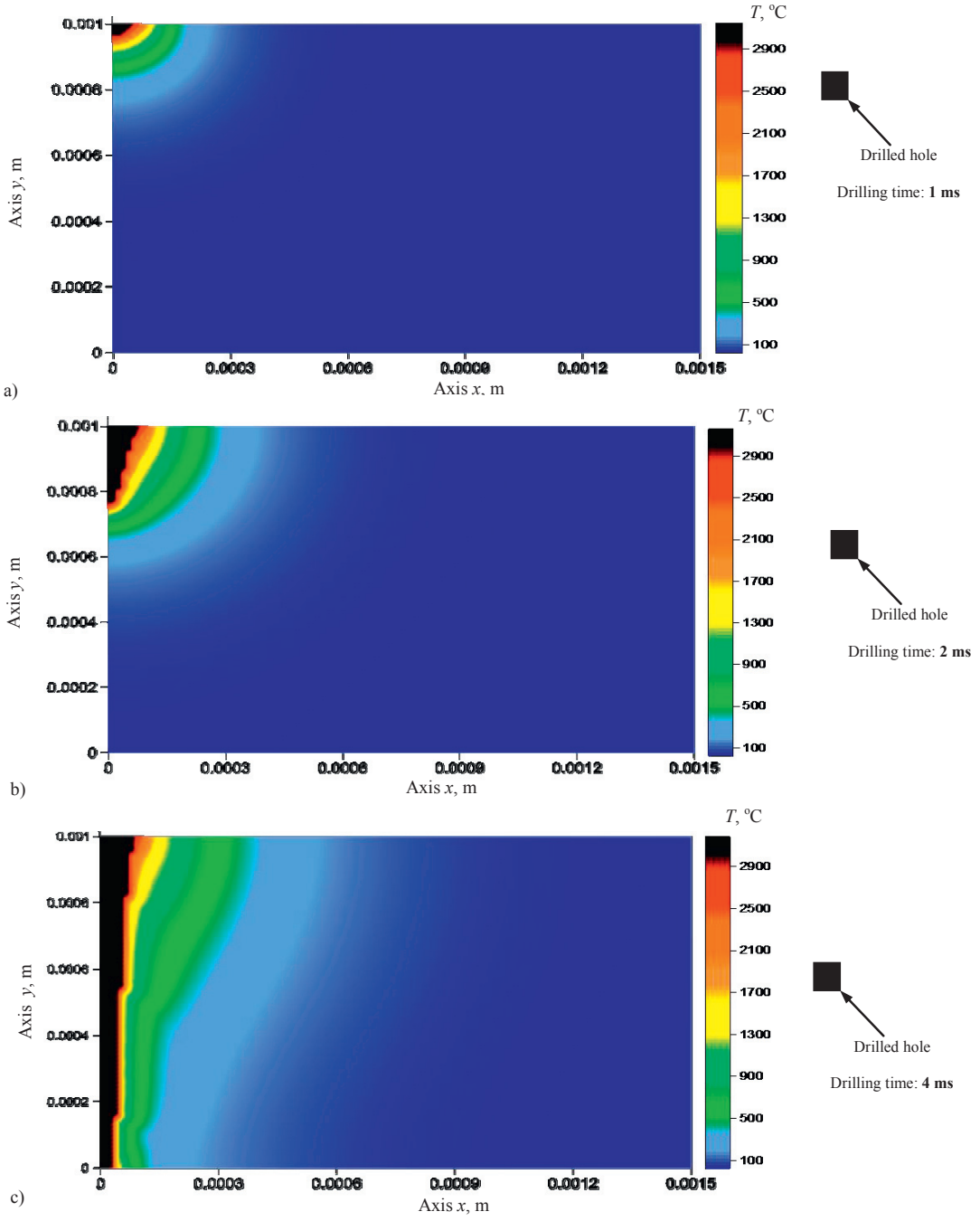

Fig. 7. Temperature distribution at different times during laser drilling.

A quantitative estimate of numerical results is performed with self-conducted experiment, as shown in Figs. 8 and 9.

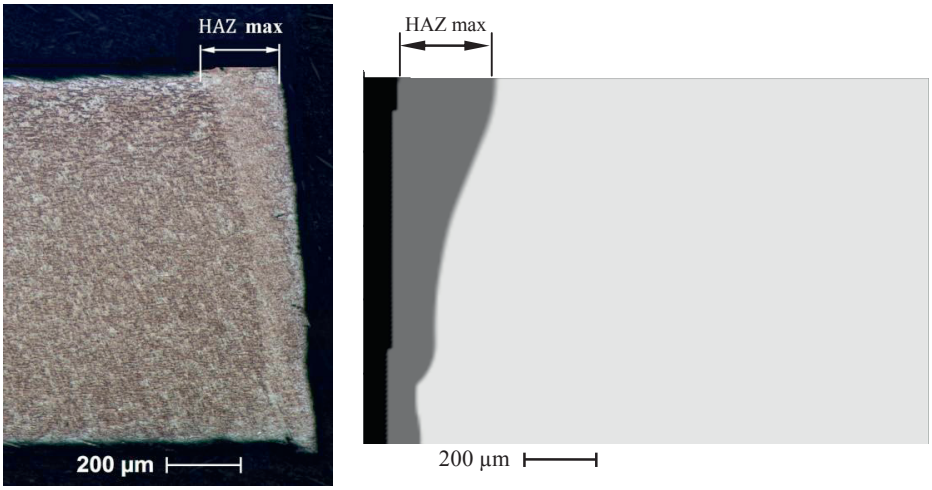

Fig. 8. The heat affected zone: experiment (left); FVM (right).

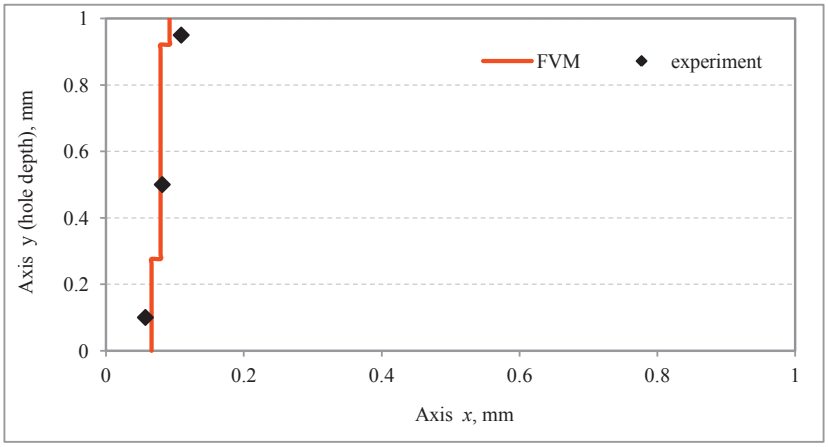

Fig. 9. The shape of hole in laser drilling process (drilling time 8 ms).

In Figs. 8 and 9 can be observed the good agreement between experimental and calculated results, the deviations are in the range of 3% to 15%. It means that the accuracy of the calculation such that the results can be used for practical purposes.

Conclusion

In this paper a finite volume based numerical method for modeling the temperature distribution to predict the heat affected zone (HAZ) and the shape of the hole during laser drilling process is successfully applied. The method solves the thermal energy balance equation written in an integral form.

The presented test cases demonstrate very good accuracy of the method. Also, the presented numerical results are compared with the self-conducted experimental results at the University of Applied Science in Jena, Germany.

The experimental results are obtained during CO_2 laser drilling of tungsten alloy sheet, thickness of 1 mm. In metallographic samples, the size of heat affected zone and the diameter of the drilled hole are measured; it is very suitable for testing the accuracy of the numerical results. Good agreement of numerical and experimental results is found.

In the future work, more detailed discussions for the effect of different parameters such as gas jet velocity, type material, and material thickness will be considered.

Acknowledgements

The authors would like to thank the Federal Ministry of Education and Science, Bosnia and Herzegovina for financial support to this study.

References

[1] A.K. Dubey, V. Yadava, Laser beam machining – A review, International Journal of Machine Tools & Manufacturing, 48 (2008) 609-628.
[2] U.C. Paek, F.P. Gagliano, Thermal analysis of laser drilling processes, IEEE Journal of Quantum Electronics QE-8, 2 (1972) 112-119.
[3] T.M. Yue, T.W. Chan, H.C. Man, W.S. Lau, Analysis of ultrasonic aided laser drilling using finite element method, Annals of CIRP 45, 1 (1996) 169-172.
[4] R.K. Ganesh, W.W. Bowley, R.R. Bellantone, Y. Hahn, A model for laser hole drilling in metals, Journal of Computational Physics, 125 (1996) 161-176.
[5] C.F. Cheng, Y.C. Tsui, T.W. Clyne, Application of a 3-D heat flow model to treat laser drilling of carbon fibre composites, Acta Metallurgica et Materialia, 46 (1998) 4273-4285.
[6] C.Y. Ho, J.K. Lu, A closed form solution for laser drilling of silicon nitride and alumina ceramics, Journal of Materials Processing Technology, 140 (2003) 260-263.
[7] D. Begic, I. Bijelonja, M. Kulenovic, A. Cekic, Numerical simulation of the laser beam drilling process, Annals of DAAAM & Proceedings of 22nd International DAAAM Symposium, 22 (2011) 0417-0418.
[8] Y.Yan, L. Ji, Y. Bao, Y. Jiang, An experimental and numerical study on laser percussion drilling of thick-section alumina, Journal of Materials Processing Technology, 212 (2012) 1257-1270.
[9] S. Mishra, V. Yadava, Modeling and optimization of laser beam percussion drilling of nickel-based superalloy sheet using Nd: YAG laser, Optics and Lasers in Engineering, 51 (2013) 681-695.
[10] S. Mishra, V. Yadava, Modeling and optimization of laser beam percussion drilling of thin aluminum sheet, Optics and Laser Technology, 48 (2013) 461-474.
[11] P. Parandoush, A. Hossain, A review of modeling and simulation of laser beam machining, International Journal of Machine Tools & Manufacture, 85 (2014) 135-145.
[12] R. Singh, M.J. Alberts, S.N. Melkote, Characterization and prediction of the heat affected zone in a laser assisted mechanical micromachining process, International Journal of Machine Tools & Manufacturing, 48 (2008) 994-1004.
[13] E. Lassner, W.D. Schubert, Tungsten – Properties, Chemistry, Technology of Element, Alloys, and Chemical Compounds, Kluwer Academic, New York, 1999.